

Detection of Spin and Orbital Magnetic Moments under Ferromagnetic Resonance

We present a microscopic investigation of spin and orbital magnetic moments (m_s and m_L) under the influence of ferromagnetic resonance (FMR), using time-resolved X-ray magnetic circular dichroism (XMCD). This technique, known as X-ray ferromagnetic resonance (XFMR), facilitates element-specific and time-resolved probing of magnetization dynamics. Recently, we established and installed an XFMR measurement system at the Photon Factory (PF). In this study, we examined the magnetization dynamics of Ni-Fe alloy thin films, and applied a Bayesian analysis to the acquired XFMR energy spectra to quantitatively evaluate the m_s and m_L in the magnetization dynamics.

The collective dynamics of spin moments, such as spin-waves, have been extensively investigated across diverse research fields for decades, holding significant promise for spintronic applications. In parallel, dynamics associated with orbital angular momentum (OAM) have recently garnered considerable attention in various research fields [1-3], because OAM is expected to play a crucial role in the advancement of both spintronic and emerging orbital devices. Direct observation of dynamic magnetic behaviors is essential to facilitate the development of spin- and orbital-momentum-based devices. One of the probes for investigating the dynamics of m_s and m_L is XMCD. This technique allows for the detection of magnetic moments along the incident X-ray direction by measuring the difference in absorption of left- and right-circularly polarized X-rays. Applying XMCD sum rules to the spectra enables quantitative evaluation of m_s , m_L , and other electronic and magnetic multipoles [4].

In this context, we have developed XFMR techniques capable of probing magnetic dynamics under the FMR effect, where GHz-range microwaves excite the magnetization precession [5]. **Figure 1(a)** illustrates the experimental setup for the XFMR system. In the PF, X-rays are injected at a frequency

of $f_0 = 500.1$ MHz in a multi-bunch mode. We utilized the synchrotron master oscillating (MO) signals, which are synchronized with the X-ray injection timing, as trigger signals to a function generator that produces higher-order radio-frequency (RF) harmonics of the X-ray repetition frequency. The magnetization precession in the sample is excited by applying the RF magnetic field via coplanar wave guide (CPW). By incrementally delaying the phase of the MO signals, the progression of magnetization dynamics can be observed. Additionally, the phase of the MO signals was modulated by π at a frequency of 1.0333 kHz using square-wave signals generated from another function generator. The square-wave signals, together with the transmitted XMCD signals, are input into a lock-in amplifier (LIA) to enhance the signal-to-noise ratio. The resulting output, referred to as the XFMR signal, reflects the difference in the X-ray absorption between opposite sides of the cone of magnetization precession. **Figure 1(b)** presents representative phase-delay scan results for a 30 nm-thick $\text{Ni}_{0.8}\text{Fe}_{0.2}$ (permalloy: Py) film acquired at the Fe L_3 absorption edge. In this measurement, an RF magnetic field at the 8th harmonic of the MO frequency ($8f_0 = 4.008$ GHz) was applied to the sample. Clear oscillatory signals with a period of approximately

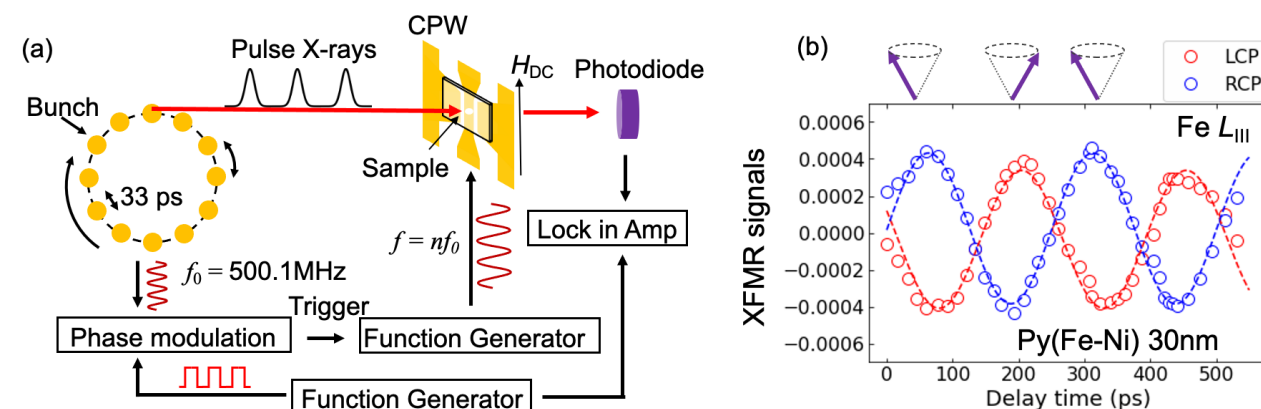


Figure 1: (a) Experimental configuration of the XFMR measurement in the PF. (b) Delay scan of XFMR signals for Py thin film. LCP and RCP represent left and right circular polarization of the incident X-rays, respectively.

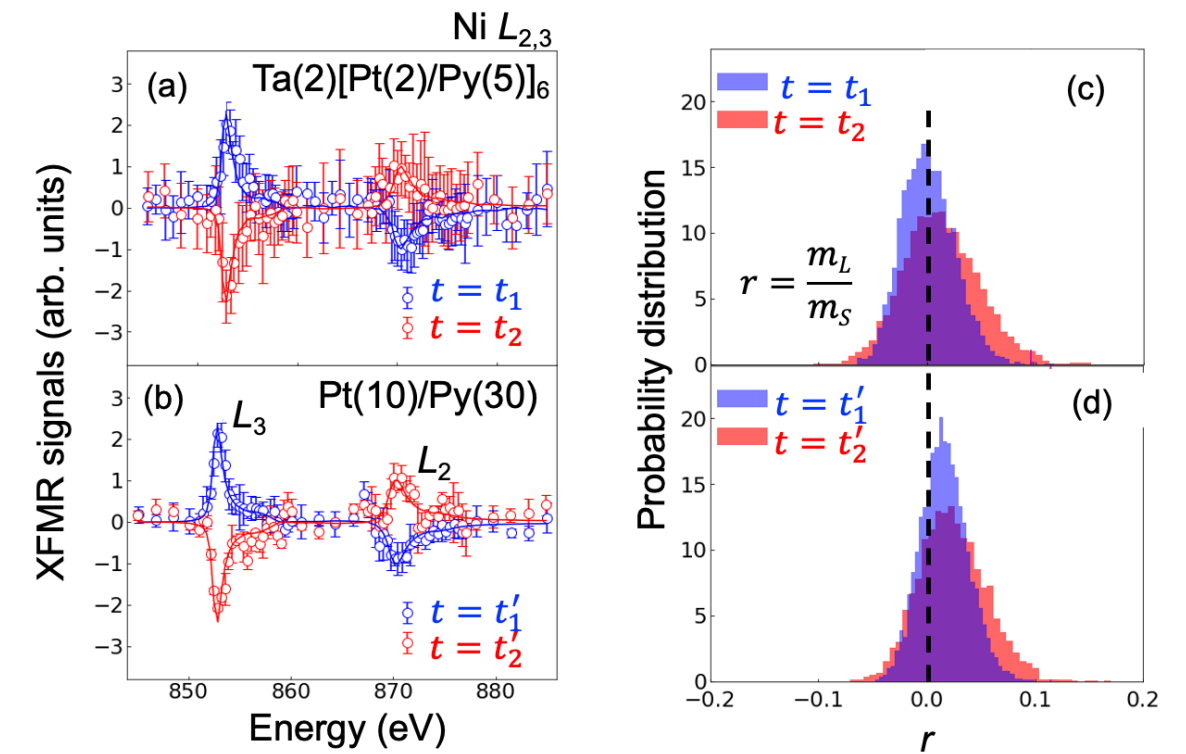


Figure 2: (a) (b) Energy spectra of XFMR signals around Ni $L_{2,3}$ edges acquired at fixed time delay, obtained from $\text{Ta(2)[Pt(2)/Py(5)]}_6$ and Pt(10)/Py(30) thin films. Red and blue lines present the estimated XFMR spectra obtained by Bayesian inference analysis. (c) (d) Posterior probability distribution of $r = m_L / m_s$. Dashed line indicates $r = 0$.

250 ps were observed. Furthermore, a phase shift of π was detected between signals obtained with left and right circularly polarized (LCP and RCP) X-rays. These results demonstrate the successful real-time detection of Fe moment precession.

To evaluate spin and orbital moment, energy spectra of XFMR signals were obtained from two types of Py multilayer systems: $\text{Ta(2)[Pt(2)/Py(5)]}_6$ and Pt(10)/Py(30) , where the values in parentheses denote individual layer thicknesses in nanometers. **Figures 2(a)** and **(b)** present the XFMR spectra around Ni $L_{2,3}$ edges acquired at fixed time delays. Well-defined spectral peaks were observed at both edges, closely resembling the features of conventional XMCD spectra. Here, we analyzed these XFMR spectra employing Bayesian analysis method to evaluate m_s and m_L in magnetization dynamics. **Figures 2(c)** and **(d)** respectively show the posterior probability distributions of the ratio $r = m_L / m_s$ for $\text{Ta(2)[Pt(2)/Py(5)]}_6$ and Pt(10)/Py(30) . The estimated r for the Pt(10)/Py(30) are slightly deviated from $r = 0$, whereas it completely disappears for the multilayered sample of $\text{Ta(2)[Pt(2)/Py(5)]}_6$. This difference may be attributed to the perpendicular anisotropy in m_L . In multilayered heterostructures composed of 3d transition metals and 5d heavy metals with significant spin-orbit coupling, m_L tends to align normal to the film surface. Such anisotropy implies a tilting of the m_L

precession axis away from the film plane, which suppresses the perpendicular dynamical component of the m_L precession in the $\text{Ta(2)[Pt(2)/Py(5)]}_6$ system.

In summary, we have developed the XFMR measurement techniques for magnetic thin film samples, enabling direct real-time observation of magnetization dynamics. Moreover, evaluation of m_s and m_L was achieved by applying Bayesian analysis to the XFMR spectra. The present techniques provide promising experimental methods for evaluation of magnetic dynamics in several types of magnetic systems.

REFERENCES

- [1] D. Go, D. Jo, C. Kim and H. -W. Lee, *Phys. Rev. Lett.* **121**, 086602 (2018).
- [2] R. R. Neumann, A. Mook, J. Henk and I. Mertig, *Phys. Rev. Lett.* **125**, 117209 (2020).
- [3] S. Ding, A. Ross, D. Go, L. Baldrai, Z. Ren, F. Freimuth, S. Becker, F. Kammerbauer and J. Yang, *Phys. Rev. Lett.* **125**, 177201 (2020).
- [4] Y. Yamasaki, Y. Ishii and N. Sasabe, *Sci. Technol. Adv. Mater.*, **26**, 2513217 (2025).
- [5] Y. Ishii, Y. Yamasaki, Y. Kozuka, J. Lustikova, Y. Nii, Y. Onose, Y. Yokoyama, M. Mizumaki, J. Adachi, H. Nakao, T. Arima and Y. Wakabayashi, *Sci. Rep.* **14**, 15504 (2024).

BEAMLINE
BL-16A

Y. Ishii and Y. Yamasaki (NIMS)